Effects beyond the random-phase approximation in calculating the interaction between metal films

J. Jung,[1] P. García-González,[2,*] J. F. Dobson,[3] and R. W. Godby[4]
[1]*Departamento de Física Fundamental, Universidad Nacional de Educación a Distancia, Apartado de Correos 60141, 28080 Madrid, Spain*
[2]*Departamento de Física de la Materia Condensada, Universidad Autónoma de Madrid, 28049 Madrid, Spain*
[3]*School of Science, Griffith University, Nathan, Queensland 4111, Australia*
[4]*Department of Physics, University of York, Heslington, York YO10 5DD, United Kingdom*
(Received 1 May 2004; revised manuscript received 20 August 2004; published 5 November 2004)

The performance of the adiabatic-connection fluctuation-dissipation theorem is discussed through the implementation of a non-local energy optimized exchange-correlation kernel to account for short-range correlation effects. We evaluate the jellium surface energy, through a painstaking extrapolation of single slab calculations, as well as the binding and interaction energies between two and three jellium slabs. Whereas *total* electron correlation energies are rather sensitive to the details of the kernel, any physically well-motivated approximation within our framework describes binding energies (including surface energies) within the same level of accuracy.

DOI: 10.1103/PhysRevB.70.205107 PACS number(s): 71.10.−w, 71.15.Mb, 71.15.Nc, 71.45.Gm

I. INTRODUCTION

In recent years there has been an increasing interest in the use of the formally exact adiabatic-connection fluctuation-dissipation theorem (ACFDT),[1] in the framework of time-dependent density functional theory (TDDFT)[2–4] to calculate electron ground-state correlation energies.[5–13] This approach, as well as formulations based on Green's function theory,[14–18] has emerged as a promising alternative to the widely used Kohn-Sham (KS) method[19] without the numerical expense of statistical diffusion quantum Monte Carlo (DQMC) or quantum-chemistry methods. In TDDFT and Green's function based methods, many of the electron correlations effects are directly built in without resorting to any mean-field-like approximation, like the widely used local density approximation (LDA)[20] or the generalized gradient approximation (GGA)[21] to the exchange-correlation energy. As a consequence, several shortcomings of the mean-field prescriptions, such as the lack of a proper treatment of long-ranged dispersion forces, can be easily overcome with these many-body approaches. Moreover, increasing computational capacity opens the appealing possibility of a unified treatment of complicated electron-electron correlations in a seamless fashion for overlapped, intermediate or distant regimes, even in systems like carbon compounds (stretched graphite, bundled nanotubes) or polymer crystals, where such dispersion forces are believed to be important. Further simplifications, which incorporate the many-body effects in an approximate but more fundamental level than KS-LDA,[22–25] might be useful in the near future to tackle very complex phenomena.

According to the ACFDT, the correlation energy of an electron system is given exactly by

$$E_C = -\int_0^{+\infty} \frac{du}{2\pi} \int_0^1 d\lambda \mathrm{Tr}(\hat{w}[\hat{\chi}_\lambda(iu) - \hat{\chi}_0(iu)]), \qquad (1)$$

where Tr is the spatial trace and the usual matrix operations are implied (we will use Hartree atomic units throughout the paper unless otherwise specified). $\chi_\lambda(\mathbf{r}_1, \mathbf{r}_2; iu)$ is the imaginary-frequency density response of a fictitious system of electrons interacting through a scaled Coulomb potential $\lambda w(r) = \lambda / r$ whose ground-state density equals the actual one, and $\hat{\chi}_0(iu)$ is the density response function of the KS non-interacting system. The latter can be evaluated exactly as follows:

$$\chi_0(\mathbf{r}_1, \mathbf{r}_2; iu) = \sum_\sigma \sum_{n,m} \frac{(f_{n,\sigma} - f_{m,\sigma})}{iu + (\varepsilon_{n,\sigma} - \varepsilon_{m,\sigma})} \times \phi^*_{n,\sigma}(\mathbf{r}_1)\phi_{n,\sigma}(\mathbf{r}_2)\phi_{m,\sigma}(\mathbf{r}_1)\phi^*_{m,\sigma}(\mathbf{r}_2), \qquad (2)$$

with $\phi_{n,\sigma}(\mathbf{r})$ and $\varepsilon_{n,\sigma}$ the KS eigenfunctions and eigenenergies with Fermi occupation numbers $f_{n,\sigma}$. In TDDFT, the density response $\hat{\chi}_\lambda(iu)$ is related to the non-interacting one by a Dyson-like matrix equation

$$\hat{\chi}_0(iu) = (\hat{1} - \hat{\chi}_0(iu)[\lambda\hat{w} + \hat{f}_{\mathrm{XC},\lambda}(iu)])\hat{\chi}_\lambda(iu), \qquad (3)$$

$\hat{f}_{\mathrm{XC},\lambda}(iu)$ being the exchange-correlation (XC) kernel of the fictitious system with the scaled interaction $\lambda\hat{w}$. Since $\hat{f}_{\mathrm{XC},\lambda}(iu)$ is unknown, practical applications of TDDFT require one to approximate such a XC kernel.

If we do not consider any XC effect in the interacting response function (i.e., we set $f_{\mathrm{XC}}=0$ thus neglecting the so-called local-field corrections), we have the random-phase approximation (RPA). The RPA treats important aspects of long-ranged correlations exactly, although it gives a poor description of short- and intermediate-ranged ones.[26] In spite of this crude assumption, the RPA accounts for dispersion forces absent in mean-field approximations,[6,8,16,27] and it seems to be a good approximation, usually better than KS-LDA or KS-GGA, for calculating binding energies.[10,13] Nonetheless, the absolute value of correlation energies is systematically overestimated, the C_6 van der Waals coefficients for some atoms are quite inaccurate,[28] and the good performance of the RPA when calculating surface energies is

very likely due to a fortunate cancellation of errors.[13] The use of simple schemes beyond RPA, like the adiabatic local density approximation (ALDA), or even more sophisticated approaches, such as the wave-function-dependent exchange-only kernel by Petersilka-Gossman-Gross,[29] does not guarantee a systematic improvement upon the RPA when calculating correlation energies and other related quantities.[5,10]

Due to the popularity of TDDFT, there is intense activity to obtain and assess better approaches to the XC kernel. They range from functional forms that rely on known properties of the homogeneous electron gas (HEG)[30–32] to truly *ab initio* schemes based on many-body techniques.[33,34] In general, these efforts have been directed toward a better description of neutral excitations, aimed at circumventing the expensive numerical implementation of the many-body Bethe-Salpeter equation.[4] However, focusing on the evaluation of correlation energies, it requires the entire knowledge of the XC kernel, including regions that are not interesting at all to obtain optical properties, Thus, the actual performance of some of these new approaches to calculate total energies is still unknown, and their sophistication might lead to unaffordable calculations when applied to real materials.

A completely different approach to this problem is the development of *energy-optimized* XC kernels, as proposed recently by Dobson and Wang.[8] Using this recipe, the XC kernel approximation is designed in such a way that the corresponding ACFDT correlation energy of a reference system (usually the HEG) fits the exact values. The main drawback of this approach is that one should not expect an overall good description of excited-state properties. However, it will lead to much better correlation energies than RPA with almost the same computational cost. On the other hand, the use of simple energy-optimized kernels could also be useful to obtain highly accurate XC potentials required, for instance, for a better performance of TDDFT approximations in the calculation of excited state properties in localized systems.

In this paper we will present a simple non-local energy-optimized XC kernel easy to implement in any RPA code. This generalizes the work of Dobson and Wang,[8] which was restricted to spatially local optimized XC kernels. Using this new kernel, we will calculate several structural properties of jellium-like systems where the ACFDT calculations are easy to carry out. More important, there is a realm of results obtained by other methods that provide a firm basis for a comparative study. In addition to this benchmark character, we will be able to analyze physical aspects that are typical of confined systems (like dissociation energies or the presence of van der Waals interactions) due to the electron localization along the z direction, while keeping the free-electron-like properties of bulk metals. Finally, we do not need to consider other factors that are important for *ab initio* studies of the properties of real materials, like the use of pseudopotentials. As a consequence, we can focus strictly on the actual performance of different approximations to the exact ACFDT-TDDFT.

II. THEORY

Since our goal is the development of a functional approximation to the XC kernel to calculate correlation energies using the ACFDT, the currently available parametrizations of the HEG XC kernel $f_{\mathrm{XC}}^{\mathrm{hom}}$ might be a promising starting point. As shown by Lein *et al.*,[7] the form developed by Richardson and Aschcroft[35] of the full dynamical HEG XC kernel leads to a perfect fit with the "exact" DQMC correlation energies. However, the same authors also found that good accuracy can be kept by using an adiabatic non-local parametrization such as the one proposed by Corradini *et al.*[30] Therefore, the dynamical features of the XC kernel have less influence than the non-locality in the correlation energy. We have checked that, as expected, this also holds for any other physically well-motivated approximation[36,37] to the static XC kernel. In addition, we have to bear in mind that there are many spectral features that could be contained in the XC kernel of an inhomogeneous system that cannot be inherited, by any means, from the homogeneous limit. Finally, naïve ways to include dynamical effects into the XC kernel can easily lead to the violation of known constraints.[38] Thus, in principle there is no need to force the frequency dependence into approximations based on functional forms of the XC kernel, if our aim is solely the evaluation of structural properties in an efficient way. Therefore, following an idea proposed several times in the literature,[31,32] we adopt the following functional approximation:

$$f_{\mathrm{XC},\lambda}(\mathbf{r}_1,\mathbf{r}_2;\omega) \simeq f_{\mathrm{XC},\lambda}^{(0)}(\tilde{n},r_{12}) = \frac{1}{\lambda} f_{\mathrm{XC}}^{(0)}\left(\frac{\tilde{n}}{\lambda^3},\lambda r_{12}\right) \qquad (4)$$

Here, the effective density $\tilde{n}$ is a function of the densities $n(\mathbf{r}_1)$ and $n(\mathbf{r}_2)$ (the arithmetical mean unless stated otherwise) and $f_{\mathrm{XC}}^{(0)}(n,r_{12})$ a certain parametrization of the static part of the XC kernel of the HEG. Of course, we recover the ALDA if we make a further approximation and neglect any non-local contribution to the HEG kernel [that is, if we set $f_{\mathrm{XC}}^{(0)}(n,r_{12}) = \kappa_{\mathrm{XC}}^{\mathrm{hom}}(n)\,\delta(r_{12})$, where $\kappa_{\mathrm{XC}}^{\mathrm{hom}}(n) = d^2[n\varepsilon_{\mathrm{XC}}^{\mathrm{hom}}(n)]/dn^2$, $\varepsilon_{\mathrm{XC}}^{\mathrm{hom}}(n)$ being the correlation energy per particle].

The encouraging results obtained by Dobson and Wang[8] using an energy-optimized ALDA suggest the construction of a simple non-local kernel that gives accurate HEG correlation energies while preserving exact limits of the actual kernel. In the HEG, the kernel $f_{\mathrm{XC}}^{(0)}(r_s,q)$ expressed in reciprocal space, is related to the static local-field factor $G(n,q)$ through the relation $f_{\mathrm{XC}}^{(0)}(n,q) = -(4\pi/q^2)G(n,q)$. The model introduced by Hubbard[39]

$$G^{\mathrm{Hub}}(n,q) = -\frac{1}{2}\frac{q^2}{q^2+q_{\mathrm{F}}^2}, \qquad (5)$$

where q_{F} is the Fermi momentum of the HEG, improves the description of short-range correlation effects reducing, in the large q limit, the Coulomb correlation between electrons of parallel spin. This was accomplished by finding an approximate way to sum all the exchange diagrams of the ladder type that entered in the evaluation of the interacting response function. This proposal inspired the elaboration of more sophisticated models along the years,[40] which turned out to be rather similar to the original model. Thus, we propose an energy-optimized Hubbard-like (OH) kernel whose expression in reciprocal space is

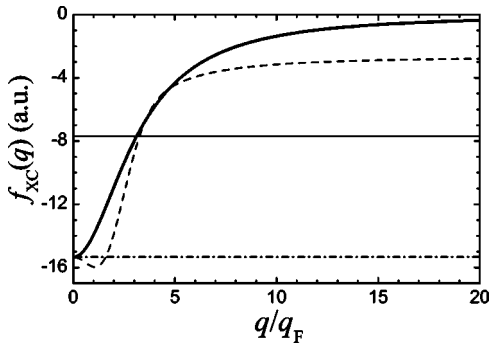

FIG. 1. Several parametrizations of the static XC kernel $f_{XC}^{hom}(q)$ of the HEG with $r_s=4$. Thick solid line: energy optimized non-local Hubbard-like kernel; thin solid line: energy optimized Dobson-Wang local kernel; dash-dotted line: ALDA; dashed line: parametrization by Corradini *et al.*

$$f_{XC}^{(0)}(r_s,q) \simeq \frac{\kappa_{XC}^{hom}(r_s)}{1+\alpha(r_s)(q/q_F)^2}, \tag{6}$$

where $r_s=[3/(4\pi n)]^{1/3}$ is the Wigner radius and $\alpha(r_s)$ is the empirical function

$$\alpha(r_s) = \frac{8.26+r_s}{100+5r_s}. \tag{7}$$

The HEG kernel (6), which is plotted for $r_s=4$ in Fig. 1, keeps the exact $q\to 0$ behavior (related to the fulfillment of the compressibility sum rule) and guarantees an excellent reproduction of the DQMC correlation energies[41] (as parametrized by Perdew and Wang[20]) for a wide range of densities (see Fig. 2). For metallic densities the relative error is negligible and the highest relative deviation (only 3%) appears

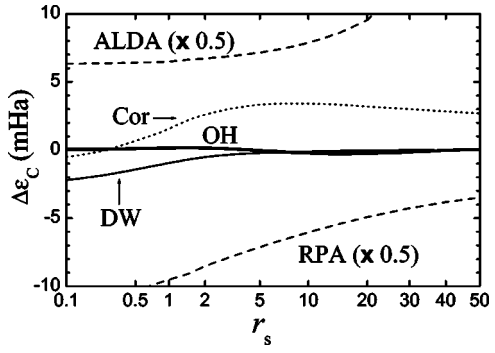

FIG. 2. The absolute error $\Delta\varepsilon_C=\varepsilon_C^{ACFDT}-\varepsilon_C^{DQMC}$ in the correlation energy per electron of the homogeneous electron gas using different XC kernels. ε_C^{DQMC} is taken from the accurate parametrization by Perdew and Wang (Ref. 20 of the DQMC data by Ceperley and Alder (Ref. 41). Note that the errors of the ALDA and RPA have been divided by two. The superior performance of the OH kernel (thick solid line) is evident for the whole range of electron densities. Note that the Dobson-Wang (DW) energy optimized prescription[8] is constructed so as to give zero absolute error $\Delta\epsilon_C$ at all r_s values, if carried out exactly. However, the simple analytic kernel given in Ref. 8 was a numerical fit to a limited range of data in the metallic range $2<r_s<5$. A better fit to the exact DW kernel could presumably be constructed for the range $r_s<2$.

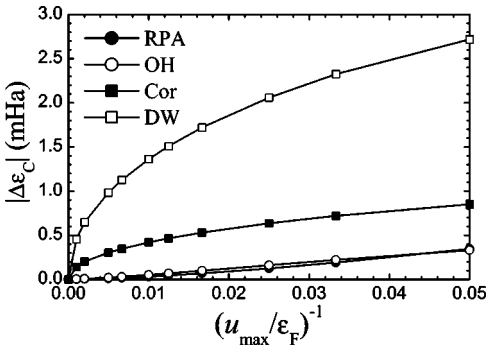

FIG. 3. The absolute convergence of the correlation energy per electron of the HEG ($r_s=4$) versus the reciprocal of frequency cutoff u_{max} in Eq. (1) for several ACFDT prescriptions (ε_F is the Fermi energy of the HEG). $\Delta\varepsilon_C$ denotes the error in ε_C relative to its converged value at $u_{max}^{-1}=0$. The excellent convergence of the RPA and OH approximations contrasts significantly with the numerical problems arising from the use of a static HEG kernel with a non-zero short wavelength term.

in the low density limit around $r_s\simeq 15$. However, we have to remember that we do not intend to present an accurate parametrization of all aspects of the XC kernel, but just a simple form suitable for accurate TDDFT total energy calculations. For instance, the proposed parametrization does not reproduce the exact behavior for $q\gg 0$ of the exact HEG XC static kernel,[37] which is a feature whose inclusion would lead to numerical problems. Indeed, any non-zero large wave vector component in a static parametrization of the kernel would also be kept in the dynamical ($iu\neq 0$) contributions to the correlation energy, hindering us from reaching quick convergence to the final ACFDT energies with respect to the cutoff u_{max} in the numerical frequency integration in Eq. (1) (see the top two curves in Fig. 3). This computational advantage of our kernel is not very important in simple systems like those treated in this work. However, it might be critical in prospective applications to real materials, since a substantial part of the computational effort might otherwise be required to calculate physically unimportant high-frequency contributions that were unnecessary using both the RPA or the optimized kernel proposed here.

III. BINDING ENERGY OF THIN METAL FILMS

As a first application of the OH kernel described in the previous section, we have calculated the total correlation energies of thin jellium metal films for several metallic densities. In all the cases, the non-interacting response $\hat{\chi}_0(iu)$ has been obtained using the KS-LDA orbitals; our tests show that the final numerical results only change marginally if we calculate χ_0 using functional models that improve upon the LDA by recovering the image-like $-1/(4z)$ behavior of the XC potential.[42] In Table I we present such energies for thin metal films with a background width of $6.4r_s$. For the optimized Hubbard kernels, we use both the arithmetical (OH1) and the geometrical (OH2) mean of the local densities to evaluate the two-point function $\tilde{n}(\mathbf{r}_1,\mathbf{r}_2)$ (of Eq. (4)). In addition, we also present the KS-LDA results, as well as the

TABLE I. Different contributions of energy per electron (in mhartree) for one isolated jellium slab of thickness $L=6.4r_s$ using the KS-LDA and the ACFDT schemes quoted in the text. Between parentheses we represent the different contributions to the binding energy per electron D_0 for a system of *two* slabs of thickness $L=3.2r_s$ at zero separation. The KS-LDA correlation energies given are the differences between the KS-LDA exchange-correlation energy and the exact exchange (EXX) energy, as explained in the text; the latter is also included in the table for comparison, as well as the KS kinetic (T_S) and total classical electrostatic (EL) energies. The numerical error bar of the RPA and OH1/2 correlation energies is 0.01 mhartree. However, due to the reasons explained in Sec. II, the uncertainties of the DW, Cor, and ALDA methods are 0.2 mhartree for the total correlation energies and 0.05 mhartree for the binding correlation energies.

		ACFDT								
r_s	KS-LDA	RPA	OH1	OH2	DW	Cor	ALDA	EXX	T_S	EL
2.0	−42.23	−58.93	−41.90	−41.86	−42.6	−39.5	−28.8	−220.55	258.18	4.07
	(2.35)	(2.56)	(2.38)	(2.42)	(2.40)	(2.40)	(2.45)	(8.72)	(−17.92)	(3.98)
3.0	−35.07	−50.62	−34.82	−34.79	−35.3	−31.9	−21.2	−148.86	117.45	1.21
	(2.08)	(2.24)	(2.13)	(2.17)	(2.15)	(2.15)	(2.20)	(3.32)	(−4.96)	(1.00)
4.0	−30.44	−45.16	−30.28	−30.25	−30.6	−27.1	−16.4	−112.44	67.13	0.55
	(1.56)	(1.72)	(1.64)	(1.68)	(1.65)	(1.65)	(1.70)	(1.83)	(−1.90)	(0.48)
5.0	−27.09	−41.16	−27.01	−26.97	−27.3	−23.7	−12.8	−90.40	43.52	0.35
	(1.22)	(1.37)	(1.29)	(1.33)	(1.30)	(1.30)	(1.35)	(1.08)	(−0.71)	(0.29)

RPA, ALDA, and optimized Dobson-Wang (DW) prescriptions of the TDDFT-ACFDT. Finally, we have also included the correlation energies given by Eq. (4) but using the parametrization of the static HEG kernel by Corradini *et al.* (Cor); this calculation will allow us to assess the actual importance of the details of the non-local parametrization used to implement the local field corrections in our ACFDT calculations. Details of the numerical procedures may be found in the Appendix.

The KS-LDA itself is a good approximation to the combined XC energy of this model system, following the usual trend of error cancellation between X and C energies even in situations where they predict values far from the exact ones.[43] Therefore, we may assess the ACFDT correlation energies through a comparison with the difference between the LDA-XC energy and the exact exchange one, calculated with the well-known expression:

$$E_X = -\int d\mathbf{r}_1 d\mathbf{r}_2 \frac{|\sum_n^{occ} \phi_n^*(\mathbf{r}_1)\phi_n(\mathbf{r}_2)|^2}{|\mathbf{r}_2 - \mathbf{r}_1|}. \quad (8)$$

We can observe that the three energy-optimized (OH1/2 and DW) approximations give very similar correlation energies (within 1 mhartree per electron), regardless of the specific details of the functional inclusion of the local field corrections. This demonstrates that the kernel optimization procedure is very robust even for these metal films, whose electron density profiles are very far from the homogeneous limit. Moreover, the total XC energies are fairly close to the LDA values, thus giving further confidence about the reliability of the optimization method. On the contrary, the non-optimized implementations of the ACFDT (RPA, Cor and ALDA) maintains the overall trend present for the HEG. Among these non-optimized approaches, the best approach is, as expected, that based on the Corradini kernel, although it overestimates the correlation energy by a few mhartree per electron compared to the energy-optimized data. Since a similar discrepancy exists for the uniform gas where the energy optimized data are the most accurate, one suspects that the energy-optimized data are superior for the inhomogeneous situation as well.

Much more relevant is the interaction energy between two metal films, since the usual KS functionals often fail to reproduce binding energies quantitatively. For two joined slabs, the binding energy per electron is given by

$$D_0 = \varepsilon_L(\infty) - \varepsilon_L(0), \quad (9)$$

where $\varepsilon_L(a)$ is the energy per electron of two slabs with thickness L at a distance a (note that $\varepsilon_L(\infty)$ is the energy per electron of a single slab with width L). The different contributions to D_0 are shown in brackets in Table I using the KS-LDA and ACFDT models for the correlation part. Note that the inclusion of local-field corrections is less relevant in this case.

The close similarity of all the OH2 results to those of OH1 indicates the insensivity to the density-averaging procedure, and in much of the rest of this paper we will not consider OH2.

For all the metallic densities, the corrections beyond the RPA (except those implemented through the ALDA) systematically lower the RPA correlation binding energy by about 5%, thus approaching the KS-LDA value. These results follow the trend anticipated by Yan *et al.*[44] about the role of non-RPA effects in the interaction between thick metal films. However these same results seem to contradict the recent findings by Pitarke and Perdew,[13] since these authors state that such effects have a marginal quantitative influence in the total surface energy [which is related to the limit $L\to\infty$ of Eq. (9)]. We will return to this issue in the next section.

In the limit of high densities the configuration of two adjacent thin slabs is not stable (that is, $D_0<0$), which is a concomitant consequence of the well-known instability of the jellium model for low values of r_s.[45,46] Nonetheless, the

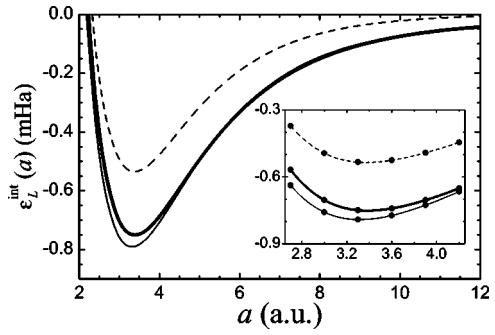

FIG. 4. Interaction energy per electron for two interacting jellium slabs of thickness $L=3a_0$ and background density $r_s=1.25$ as a function of the distance a. The inset shows in more detail the binding curve around the mechanical equilibrium distance. Thick solid line: OH1; thin solid line: RPA; dashed line: KS-LDA. We can see how the KS-LDA underestimates the binding energy, whereas the RPA predicts a smaller bond-length than the OH1 and KS-LDA.

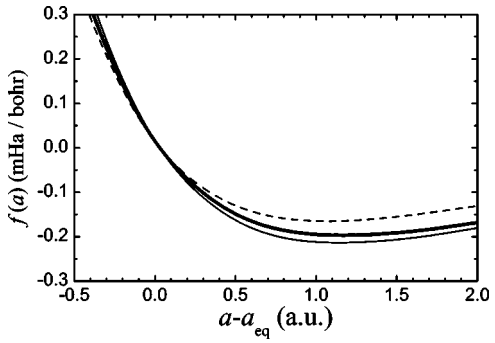

FIG. 5. As in Fig. 4, but representing the interaction force per electron. Whereas the three models behave similarly if $a<a_{eq}$, the KS-LDA deviates from the ACFDT results if $a>a_{eq}$.

two jellium interacting films will be at mechanical equilibrium at a distance a_{eq}, where the interaction energy curve between the slabs $\varepsilon_L^{int}(a)=\varepsilon_L(a)-\varepsilon_L(\infty)$ reaches a minimum. To analyze the role played by the local-field corrections, we will compare the equilibrium properties for two films with a background density $r_s=1.25$ and thickness $L=3a_0$ using the RPA and the OH1.

For this model system, the binding energy per electron $D=-\varepsilon_L^{int}(a_{eq})$ given by the RPA (see Fig. 4 and Table II) is far greater than the KS-LDA one, and slightly larger than that obtained through the OH1 method. Hence, we have a similar trend as in the case of two slabs at zero separation (and hence out of equilibrium), but now the differences between the KS-LDA and the ACFDT methods are more important. Interestingly, the KS-LDA and OH1 equilibrium distances are practically the same, but the RPA underestimates a_{eq} by more than 2%. That means that the absence of local field corrections tends to reduce the bond length between the slabs, a tendency already observed by Fuchs and Gonze for the Be_2 dimer.[10] Finally, there are significant differences in the elastic constant per particle, that we define as $C_\perp=d^2\varepsilon(a)/da^2$ (at $a=a_{eq}$): the RPA value is about 10% larger than OH1, whereas the KS-LDA is a similar amount smaller. The poor performance of the LDA for the binding energy here continues a trend noted by Dobson and Wang[47] for the LDA layer-layer binding energy to be worse for lower r_s values. The error is worse here than for the regular metallic densities ($2<r_s<6$) treated by Dobson and Wang, and constitutes a significant failing of the LDA. As an illustrative fact, the interaction energy curve is not binding when the non-local exact exchange is combined together with the LDA correlation energy, suggesting that energy functionals with similar precision should be used for the exchange and correlation energies. This means that the interaction energy given by the LDA correlation energy is far too small compared to the non-local results whereas the LDA exchange, which is more binding than the exact exchange, cannot compensate for this failure. While the LDA usually predicts overbinding in molecules[10] it is remarkable to find this opposite behavior for the binding between the slabs. This fact indicates that the LDA will be specially unsuitable in regions where the weak non-local dispersion forces are more relevant than in usual atomic or molecular systems. The GGA has also been shown to be insufficient for describing layer-layer interaction energies when long-ranged effects play an important role.[25]

TABLE II. Mechanical equilibrium properties (see the text) of two interacting jellium slabs of thickness $L=3a_0$ and $r_s=1.25$ obtained using the KS-LDA, the ACFDT-RPA, and the ACFDT-OH1. Note the coincidence between the KS-LDA and the OH1 equilibrium distance.

	a_{eq} (bohr)	D (mhartree)	$C_\perp$ (mhartree/bohr^2)
KS-LDA	3.38	0.53	0.45
RPA	3.32	0.79	0.55
OH1	3.38	0.75	0.49

The KS-LDA not only fails to describe the bonding energy around the equilibrium distance, but also in the limit of higher separations. If $a>a_{eq}$, the covalent bond between the slabs ceases to exist and van der Waals (vdW) dispersion forces play a prominent role. In this case, the non-local effects are manifest and the KS-LDA behavior clearly fails. This effect can be seen very clearly in the tail of Fig. 4, but also in Fig. 5, where we represent the interaction force per electron $f(a)=-d\varepsilon_L(a)/da$ for this model system. If $a<a_{eq}$, where the films tend to repel each other, the three approximations show the same performance. However, if $a>a_{eq}$ the LDA underestimates the attractive force between the films. It is worth noting that, as before, the inclusion of a non-local f_{XC} partially compensates for the difference between the RPA and the KS-LDA.

It is very likely that the general trends we have described in this section will also be valid for real layered materials (like BN or graphite), as suggested by Dobson *et al.*[27] through an estimation of the many-body corrections to the interacting energy between layers in bulk graphite. Nevertheless, it is important to point out that the RPA might overcorrect the local density results. In this respect, the sophisticated XC functional approximation by Rydberg *et al.*,[25] which is constructed such that the long-distance vdW forces are incorporated in a seamless way, seems to underestimate the binding energy and the elastic constant of graphite (considering

the experimental uncertainties). In real layered systems there is a delicate combination of trends that results from the existence of local atomic bonds and weak dispersion forces. Then, it is very unlikely that a KS calculation, even with very elaborate functional approximations, would be able to describe these situations properly, where several phenomena characterized by different length scales co-exist. A full many-body analysis of the structural properties of such real systems is a challenge for the immediate future. While the many-body methods incorporate more clearly the relevant physical features the technical subtleties associated with these calculations may be even more delicate than those of the current approach. Total energy calculations based on many-body perturbation theory either in the GW approximation or derived from Luttinger-Ward functionals along with their self-consistent conserving extensions open a promising field for future research for describing real materials.

IV. SURFACE ENERGIES

In a series of important papers,[5,13,48] Pitarke and coworkers have given further insight into the long-standing puzzle of the surface energy of simple metals. Their findings suggest that the deviations of the statistical DQMC[49] and Fermi hypernetted chain[50] calculations from the KS-LDA surface energies could be due to inconsistencies in the extrapolation procedures required to infer the values associated with a semi-infinite geometry from finite-size calculations, as well as in the comparison between the energies of the inhomogeneous system and the HEG. As a consequence, the KS-LDA jellium surface energies may be considered as a fairly good approximation to the (still unknown) exact values. The results presented in Sec. III, as well as qualitative analysis made, among others, by Yan *et al.*[44] indicate that such exact values would lie between the LDA and the RPA. Pitarke and Perdew[13] have recently shown that the RPA correlation surface energy exhibits a clear cancellation of errors between low- and high-$q_\parallel$ contributions ($\mathbf{q}_\parallel$ is the component of the momentum parallel to the surface). Strikingly, by including the local-field correction using the Corradini kernel, they found that such cancellation is almost complete. Therefore, their estimation of the surface energies is much closer to the RPA than to the LDA. Without questioning at all the physical arguments reported by Pitarke and Perdew, we note that these conclusions, about the role played by the local-field effects, do not follow the general trends presented in Table I. However, as we mentioned in Sec. II, the static Corradini kernel has a physical finite short wavelength contribution that dominates over the bare Coulomb potential $4\pi/q^2$, leading to ACFDT calculations that are much harder to converge than the conventional RPA ones. Since surface energies are very delicate quantities, a painstaking analysis of the results is required.

The correlation contribution to the jellium surface energy can be written as

$$\sigma_C = \lim_{L\to\infty} \sigma_C(L), \tag{10}$$

with the finite-size correlation surface energy $\sigma_C(L)$ given by[51]

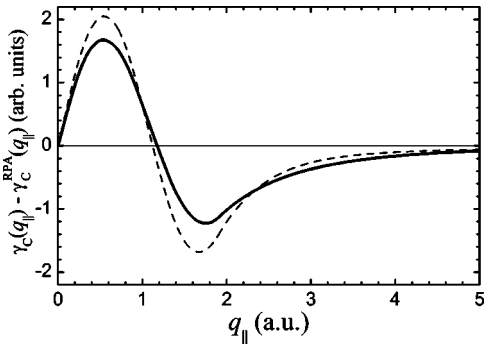

FIG. 6. Local-field corrections to the $q_\parallel$-dependent distribution $\gamma_C(q_\parallel) - \gamma_C^{RPA}(q_\parallel)$ for a jellium slab of thickness $L = 12.52 r_s$ ($r_s = 2$). Solid line: OH1, dashed line: Cor.

$$\sigma_C(L) = \int_{-\infty}^{+\infty} dz_1 dz_2 \int_0^{+\infty} dq_\parallel \exp(-q_\parallel z_{12}) \times \int_0^{+\infty} \frac{du}{4\pi}\left[\frac{n(z_1)}{n}\Delta\chi^{\text{hom}}(z_{12}) - \Delta\chi(z_1,z_2)\right] \equiv \int_0^{+\infty} dq_\parallel \gamma_C(q_\parallel) \equiv \int_0^{+\infty} du \zeta_C(iu).$$

Here, $z_{12} \equiv |z_1 - z_2|$, L is the thickness of a jellium slab with background density n, and $n(z)$ is the electron local density. To simplify the notation, we have not included the dependence on u and $q_\parallel$ into the inhomogeneous (χ) and homogeneous (χ^{hom}) response functions, and we have defined the operator

$$\Delta\hat{\chi} = \int_0^1 d\lambda (\hat{\chi}_\lambda - \hat{\chi}_0).$$

In Figs. 6 and 7 we plot the differences between the RPA distributions $\gamma_C^{RPA}(q_\parallel)$ and $\zeta_C^{RPA}(iu)$ and those corresponding to an ACFDT calculation using the OH1 and Cor f_{XC}

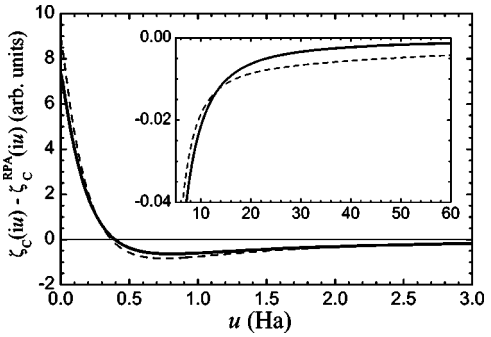

FIG. 7. Local-field corrections to the frequency-dependent distribution $\gamma_C(iu) - \gamma_C^{RPA}(iu)$ for a jellium slab of thickness $L = 12.52 r_s$ ($r_s = 2$). Solid line: OH1, dashed line: Cor.

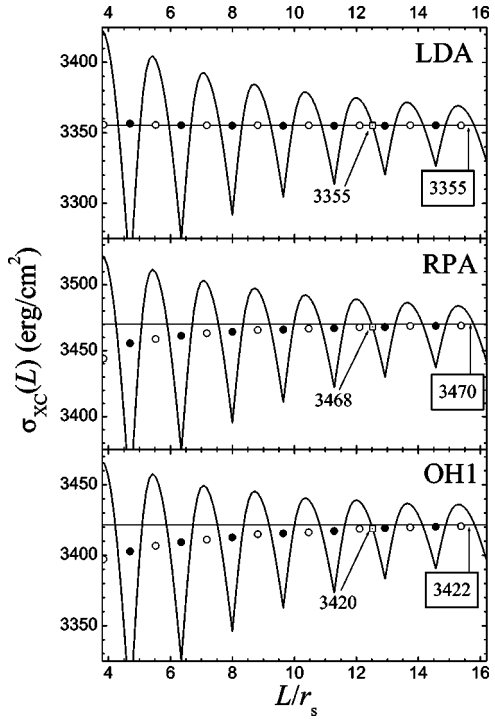

FIG. 8. The finite-size XC surface energy for $r_s=2$ using the KS-LDA, RPA, and OH1 approximations. The open circles represent the averages over each oscillation, whereas the closed circles are the estimations of the surface energy following the procedure by Pitarke and Eguiluz (Ref. 5). In each panel, the hollow square marks the single slab geometry ($L=12.52r_s$) used to estimate the local field corrections to the RPA.

functionals for a jellium slab with $r_s=2$ and thickness $L=12.52a_0$. At a first glance there are not qualitative differences between both ways to include local-field corrections. We may observe that the OH1 $q_\parallel$-distribution is slightly closer to the RPA than is the Cor one except in a region around $q_\parallel \simeq 3.5$, but in both cases the cancellation of low and intermediate $q_\parallel$ local-field corrections is evident. The same holds for the decomposition in imaginary frequencies (Fig. 7) since small u-dependent local field corrections tend to increase the surface energy, but this is compensated by contributions from higher u. However, as we may see in the inset in Fig. 7, due to the reasons explained in Sec. II, the function $\zeta_C^{\mathrm{Cor}}(iu)$ decays very slowly. Whence, small numerical uncertainties in the treatment of this high-u region might be the origin of a certain overestimation of the ACFDT-Cor correlation surface energies.

To confirm this possibility, we have calculated the local-field corrections to the exchange-correlation surface energy through the OH1, OH2, and Cor functional approximations. Note that we do not need to make a fully converged calculation of σ_{XC} for each case, but just of the difference $\sigma_{\mathrm{XC}}-\sigma_{\mathrm{XC}}^{\mathrm{RPA}}$.[52] This can be done through a systematic elimination of possible sources of error, as we may see in Fig. 8. The finite-size approximation to the XC surface energy $\sigma_{\mathrm{C}}(L)$ exhibits clearly defined regions limited by the onset of the occupancy of a new z-subband. A way to find the limit $L\to\infty$ of $\sigma_{\mathrm{XC}}(L)$ is the evaluation of the mean value in each oscillation. An alternative is the Pitarke-Eguiluz extrapolation procedure,[5] which makes use of values taken from two consecutive oscillations. Both methods give the same results but, whereas they converge extremely fast under the KS-LDA, the ACFDT finite-size energies reach the infinity limit more slowly. Fortunately, as may be inferred from the data represented in Fig. 8, the differences between the RPA and the OH1 energies are very stable as a function of the slab thickness L. As a consequence, by choosing only one suitable geometry we can calculate the difference $\sigma_{\mathrm{XC}}-\sigma_{\mathrm{XC}}^{\mathrm{RPA}}$ with very high precision. We take a slab whose KS-LDA finite-size XC surface energies equal the corresponding infinite limit and then we calculate the difference between the RPA and the OH1 energies. Although they do not match the infinite width limits separately, the difference does. Presuming that the same reads for the OH2 and Cor functional approximations, we can fairly predict the correction to the RPA energy. We have chosen a geometry with eight occupied z-subbands, which gives us a balance between size-convergence and numerical ease, since the wider the slab the more difficult to converge the ACFDT calculation. Nonetheless, even with these precautions, the numerical uncertainty of the ACFDT-Cor is many times greater than the OH1 and OH2 ones.

Our results are presented in Table III, where we also show the KS-LDA, KS-MGGA,[44] and our converged RPA XC energies, the latter being practically identical to that reported

TABLE III. The ACFDT and KS exchange-correlation contributions σ_{XC} to the jellium surface energy, in erg/cm^2. An estimation of the numerical uncertainties of our ACFDT values is also shown, as well as the width of the slab (between parentheses in units of r_s) used to evaluate the local field corrections to the RPA energies. Note how such local field corrections systematically shift down the RPA surface energies, although they do not reach the predictions from a mixed RPA+GGA calculation. The values corresponding to the RPA+GGA (see the text) and the KS−MGGA have been extracted from Ref. 44. All the results have been obtained from self-consistent LDA wave functions.

r_s	$\sigma_{\mathrm{XC}}^{\mathrm{KS-LDA}}$	$\sigma_{\mathrm{XC}}^{\mathrm{RPA}}$	$\sigma_{\mathrm{XC}}^{\mathrm{OH1}}$	$\sigma_{\mathrm{XC}}^{\mathrm{OH2}}$	$\sigma_{\mathrm{XC}}^{\mathrm{Cor}}$	$\sigma_{\mathrm{XC}}^{\mathrm{RPA+GGA}}$	$\sigma_{\mathrm{XC}}^{\mathrm{KS-MGGA}}$
2.0 (12.52)	3355	3470±2	3422±2	3435±2	3440±20	3415	3402
2.3 (12.65)	2019	2099±1	2066±1	2075±1	2075±20	2061	2048
3.0 (12.84)	764.1	803±1	788±1	793±1	795±10	783	779
4.0 (13.01)	261.5	279.0±0.5	273.0±0.5	276.0±0.5	277±5	269	266
5.0 (13.11)	111.1	119.5±0.5	116.5±0.5	118.5±0.5	119±5	113	113

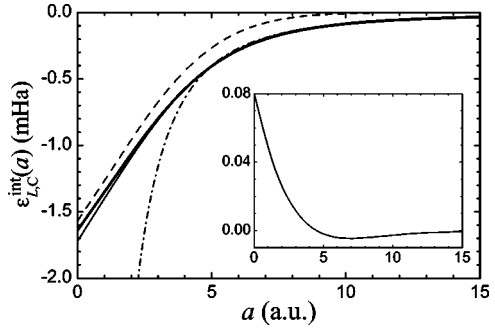

FIG. 9. Correlation contribution to the interaction energy for two jellium slabs of thickness $L=12.8$ a.u. and background density $r_s=4$, as a function of the distance a. Thick solid line: OH1; thin solid line: RPA; dashed line: KS-LDA. The latter, obtained by subtracting the exact exchange energy from the KS-LDA exchange-correlation one, goes very quickly to zero. The ACFDT results exhibit a clear power-law decay (the fitted power is $p=5/2$) which reflects the existence of long-distance vdW forces. We also plot the numerical fit (dashed-dotted line) described in the text of the OH1 results obtained from values between $a=20$ and $a=25$. The inset shows the difference between the OH1 and RPA energies, which decays as $a^{-7/2}$.

by Pitarke and collaborators.[5,13] We have also included the results obtained from the addition of a GGA functional to the ACFDT-RPA.[44] We can see that *all* the ways to include local-field corrections lower the RPA XC surface energy, thus following the trend we found for thinner slabs. Moreover, the surface energies are rather insensitive to the details of the functional form of f_{XC}. However, the corrections based on the hybrid RPA+GGA prescription are greater than the fully ACFDT ones, especially for lower densities. Thus, the main conclusions reached by Pitarke and Perdew in Ref. 13 are confirmed: surface energies are closer to the RPA ones than previously expected and the accuracy of the RPA is due to a systematic cancellation of errors. The small, but in principle relevant, differences between our Cor results and those reported before[13] should be solely attributed to the difficulties of such an ACFDT calculation.

V. van der WAALS DISPERSION FORCES BETWEEN METAL FILMS

To close the analysis that we are presenting on the influence by local-field corrections on correlation energies, we present in this section several results concerning the interaction force between simple jellium films at large separation. As has been stated before many times,[6,8,16,27] this limit shows a genuine manifestation of long-ranged correlation effects through the appearance of van der Waals dispersion forces. Then, when the electron densities of each film have an exponentially small overlap, the interaction energy $\varepsilon_{L,C}^{\mathrm{int}}(a)$ still takes a non-zero value. We have already shown this fact in Fig. 4, and it can be seen in Fig. 9 as well.

Such long-distance behavior can be explained in terms of the coupling between two-dimensional (2D) collective modes confined in each metal film.[27] Therefore, local-field effects would be only important in the limit $a \gg 0$ if they led to a correction of the $q_{\parallel} \to 0$ contributions to the correlation energy. This is not the case, since in this limit the bare Coulomb potential dominates, and the leading term of the asymptotic behavior of $\varepsilon_{L,C}^{\mathrm{int}}(a)$ must be the same for all the ACFDT prescriptions. Indeed, as we may see in Fig. 9, the differences between the RPA and OH1 approximations are relevant only in the limit of short separations (already discussed in Sec. III). In this limit, the local field corrections shifts the binding curve up very slightly, making it closer to the KS-LDA one. By using their energy optimized local kernel,[8] Dobson and Wang obtained the very same trend which also appears in many-body GW calculations of the total energy of a similar model system.[16]

Besides these qualitative considerations, we can provide further insights about the long-distance energy interaction between conducting films. Its asymptotic form can be written as

$$\varepsilon_{L,C}^{\mathrm{int}}(a) \approx -\frac{C}{(a+b)^p}, \tag{11}$$

with fitting constants C, b, and p. Electron hydrodynamic theory, which properly takes into account the main geometrical features of the problem, predicts a value $p=5/2$ for thin metallic slabs and $p=2$ for semi-infinite metals.[27] In the limit of infinite separation, Sernelius and Björk confirmed the $p=5/2$ power-law decay after a RPA calculation for a pair of perfectly 2D quantum wells.[53] Hence, for our fully microscopic calculations, we must expect the $p=5/2$ decay as well. To numerically obtain the values in the asymptotic form (11), we have sampled energy values corresponding to separation distances within the range [20, 25] bohr. However, any fixed value of p between 2.0 and 2.5 guarantees a perfect fit in this range. Nonetheless, only a value very close to 2.5 also yields an equally excellent fit *outside* the mentioned fitting region, including those corresponding to distances up to $a=50$ a.u. As a consequence, we have assumed the power decay $p=5/2$, and this is the asymptotic behavior plotted in Fig. 9. As expected, the RPA and OH1 interaction energies share the same dominant behavior $C=32.5\pm0.5$ mhartree $\times$ bohr$^{5/2}$ for the considered geometry (two slabs of thickness $L=12.8$ a.u., and mean density $r_s=4$). The local field corrections only affect the constant b, which takes the values 0.9 and 0.8 a.u., respectively. That is, within the numerical precision of our calculations, beyond RPA effects yield a 10% change over the second-order term of the long-distance interaction between these metal films.

Although not the main focus of this work, it is interesting to close this section with a brief discussion on the non-linear terms appearing in three-body interactions. For complex systems made up of several interacting systems, it has been traditional to calculate the long-ranged dispersion energy approximately as a sum of pairwise contributions retaining only the leading term corresponding to a two-body system. Thus, higher order non-additive terms of the interaction between more than two bodies are neglected. Although in a different context, a paradigmatic example for this non-additive behavior is the Axilrod-Teller-Muto[54] triple-dipole dispersion interaction term in a system of three distant neu-

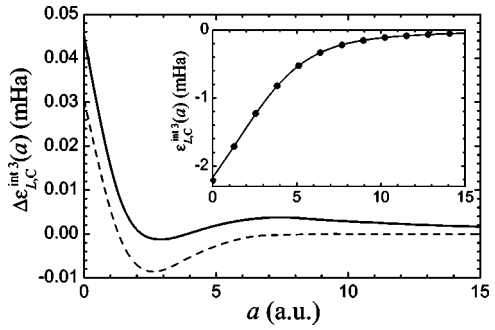

FIG. 10. The non-additive difference $\Delta\varepsilon_{L,C}^{int3}(a)=\varepsilon_{L,C}^{int3}(a)-\varepsilon_{L,C}^{int3w2}(a)$ between the correlation contributions to the interaction energy per particle for three equally spaced slabs ($L=12.8$ a.u. and $r_s=4$) as calculated from a full three-body calculation and from two-body interactions (3w2). Solid line: ACFDT-OH1, dashed line: KS-LDA. For distances less than 5 a.u. the differences are mainly due to the distinct overlapping in the two- and three-slab systems. However, if $a\gtrsim 7$ such differences are only due to the the presence of non-additive terms in the actual dispersion forces for the three-slab system. The inset shows the total correlation contributions $\varepsilon_{L,C}^{int3}(a)$ (solid line) and the additive part $\varepsilon_{L,C}^{int3w2}(a)$ (dots) using the ACFDT-OH1.

tral atoms. This term depends on the relative angle formed by the three atoms taking a positive repulsive value for a triangular shape, but a negative attractive one for the linear disposition. In order to study the pairwise non-additivity of the jellium slabs energy we have carried out the calculation of *three* slabs, of equal thickness L and equal spacing a, as a function of a, that will be compared to the sum of energies for pairs of slabs.

The additive part of the correlation $\varepsilon_{L,C}^{int3}(a)$ to the interacting energy per electron of a three-slab system obtained from the results $\varepsilon_{L,C}^{int}(a)$ of two interacting slabs may be written as

$$\varepsilon_{L,C}^{int3w2}(a)=\tfrac{2}{3}(\varepsilon_{L,C}^{int}(2a+L)+2\varepsilon_{L,C}^{int}(a)). \qquad (12)$$

The first term on the right-hand side accounts for the interaction between the farthest external slabs, while the second term describes the two interactions between the closest pairs. The factor 2/3 is included to correctly compare the energy per electron of systems with different number of slabs. The residual, non-additive, part is shown in Fig. 10, and is largest for small separation distances. However, this should be attributed to the fact that the energies are being evaluated on different overlapping electronic density profiles. In fact, the energy differences shown in Fig. 10 stabilize at a distance $a\gtrsim 7$, where the electron overlapping is very small. Then, we can see unambiguously the non-additive effects which, of course, are not present in a KS-LDA calculation. Using the ACFDT-OH1 approximation, such non-additive effects lead to a decrease of the attractive force at large distances and, within our numerical error bars, lowering by about 10% the absolute value of the leading asymptotic term from the additive 3w2 expression. It would be interesting to obtain a further confirmation using, for instance, a model calculation as that carried out in Ref. 53 due to the implications that this result might have for simplified descriptions of the interaction forces in complex layered systems.

VI. CONCLUSIONS

In this paper we have presented a static functional approach to the XC kernel of arbitrary inhomogeneous systems based on a non-local parametrization of the HEG XC kernel constructed via an energy optimization procedure. This way to introduce local field corrections seems to be a very robust procedure, since the correlation energies obtained are very similar regardless of the specific details of the functional construction. To test this prescription, we have calculated ACFDT correlation energies for highly inhomogeneous systems, interaction energies between metal films, simple metal surface energies, and analyzed long-distance correlation vdW forces.

As a general trend for these systems, local-field corrections correct the RPA results, shifting them toward the KS-LDA values. Very likely such corrections are less important than those expected previously from the modeling of effects beyond RPA using local or semilocal prescriptions.[44] This is specially manifest in the case of jellium surface energies, where our full ACFDT result lies between the RPA values and the hybrid RPA+GGA ones that, until now, could be considered as the best approach to the exact surface energies.

This work provides a firm basis to the use of energy optimization procedures for prospective applications of the TDDFT-ACFDT, but there are several important points that deserve future attention. The first one is the self-consistency issue, since so far all the TDDFT and many-body calculations of correlation energies have been carried out over KS density profiles. In other words, the set of one-electron wave functions does not minimize the total energy expression that contains the ACFDT correlation. Important steps have already been taken in this direction,[55,56] but a fully (or, at least, partially) self-consistent implementation of the TDDFT-ACFDT at a numerically affordable cost is clearly an attractive challenge. For the model systems treated in this paper, it is very unlikely that self-consistency would be important. However, it would not be the case for many localized systems and, of course, for any other problem where the KS-LDA or GGA is not an optimal approach to the exact KS non-interacting system.

A second issue that we would like to emphasize in these conclusions is related to the functional approximation to the XC kernel itself. There are limits that are not recovered by the simple Hubbard-like form we have used here. For instance, the XC-kernel so constructed lacks the inclusion of self-interaction corrections for one- or two-electron systems. That means that the energy-optimized functional forms must be improved to properly account for this limit, which definitely might be important in systems with highly localized electrons. Work is currently in progress to include such self-interaction corrections while keeping the numerical stability of the functional approximation.

ACKNOWLEDGMENTS

The authors gratefully thank J. E. Alvarellos, E. Chacón, K. T. Delaney, T. Gould, J. M. Pitarke, A. Rubio, S. Tsuzuki,

and U. von Barth for many valuable discussions. This work was funded in part by the EU through the NANOPHASE Research Training Network (Contract No. HPRN-CT-2000-00167) and the Spanish Education Ministry DGESIC grant BFM2001-1679-C03-03.

APPENDIX: NUMERICAL PROCEDURE

For a spin-compensated system exhibiting translational invariance along the *XY* plane, the KS orbitals and energies are $\phi_{n\mathbf{q}_\parallel}(\mathbf{r})=\psi_n(z)\exp(i\mathbf{q}_\parallel\cdot\mathbf{r}_\parallel)/(2\pi)^2$ and $\varepsilon_{n\mathbf{q}_\parallel}=\varepsilon_n+q_\parallel^2/2$. $\psi_n(z)$ and ε_n are the solution of the reduced eigenvalue problem

$$\left[-\frac{1}{2}\frac{\partial^2}{\partial z^2}+v_S(z)\right]\psi_n(z)=\varepsilon_n\psi_n(z) \tag{A1}$$

where $v_S(z)$ is the KS effective potential. Then, all the relevant operators can be written in a representation on the coordinates $z_{1,2}$ and the *XY* relative distance $r_\parallel=|\mathbf{r}_{\parallel,1}-\mathbf{r}_{\parallel,2}|$ (or, equivalently, on the modulus $q_\parallel$ of the *XY* momentum). Thus, the ACFDT correlation energy per surface unit can be written as

$$\frac{E_C}{S}=-\int_0^{+\infty}\frac{du}{2\pi}\int_0^{+\infty}dq_\parallel e_C(q_\parallel,u), \tag{A2}$$

where

$$e_C(q_\parallel,u)=\int dz_1dz_2e^{-q_\parallel|z_1-z_2|}\times\left[\int_0^1\chi_\lambda(z_2,z_1,q_\parallel;iu)d\lambda-\chi_0(z_2,z_1,q_\parallel;iu)\right]. \tag{A3}$$

For each $q_\parallel$ and u, we evaluate the non-interacting response χ_0 and obtain the interacting one χ_λ solving the Dyson equation (3). The λ dependence is represented by an eighth-order Gauss-Legendre (GL) grid, which is ample because of the smooth dependencies on the scaling parameter λ. The $q_\parallel$ points are distributed in two GL grids (each one typically comprising 30–40 points). The first grid includes small values of the momentum, and the second one is a coarser grid for the high momentum contributions up to a value $q_{max}\simeq 30q_F$, q_F being the Fermi momentum of the HEG with the averaged density n of the slabs. The frequency u is described in a similar fashion, with the coarse grid reaching the cutoff value $u_{max}\simeq 40q_F^2$. Nonetheless, as mentioned in Sec. II, u_{max} must be increased several times to reach a good convergence if using DW or Cor kernels. In any case, to reduce numerical uncertainties like those shown in Fig. 3, high-u asymptotic contributions are estimated by numerical extrapolation.

The non-interacting response χ_0 can be obtained from an infinite sum over all (occupied and unoccupied) z-dependent KS orbitals $\psi_m(z)$:

$$\chi_0(z_1,z_2,q_\parallel;iu)=\sum_n^{occ}\psi_n(z_1)\psi_n(z_2)\times\sum_m S_{nm}(q_\parallel,iu)\psi_m(z_1)\psi_m(z_2), \tag{A4}$$

where $S_{nm}(q_\parallel,iu)$ are analytical functions.[57] In this case, the number of unoccupied states in Eq. (A4) is a critical parameter, and the convergence must be then carefully checked. Typically, about 150 (250) z states are needed to reach the required accuracy for thin slabs (surface energies) calculations. Since the KS wave functions themselves are not an optimal representation of the density response, we solve the Dyson equation ((3)) for each u, $q_\parallel$, and λ using a representation in an orthogonal set of N_B functions of the sub-space generated by the product functions $\psi_n(z)\psi_m(z)$.

A way to circumvent the infinite sum appearing in Eq. (A4) is the use of the Green function $G(z_1,z_2;\Omega)$ of the reduced z-dependent KS Hamiltonian (A1) to evaluate the non-interacting response.[58,59] In this scheme, the interacting response is evaluated by solving directly (3) in its z representation. The second method, if enough care is taken, is exact up to the numerical errors due to the discretization of the z space, which is actually the only critical convergence parameter. The choice $dz=0.05r_s$ is enough to reach converged results. We have followed both procedures as a further check of the numerical accuracy of our results.

*Present address: Departamento de Física Fundamental, Universidad Nacional de Educación a Distancia, Apartado de Correos 60141, 28080 Madrid, Spain

[1] D. C. Langreth and J. P. Perdew, Solid State Commun. **17**, 1425 (1975); Phys. Rev. B **15**, 2884 (1977).
[2] E. Runge and E. K. U. Gross, Phys. Rev. Lett. **52**, 997 (1984).
[3] E. K. U. Gross, J. F. Dobson, and M. Petersilka, in *Density Functional Theory II*, edited by R. F. Nalewajski (Springer, Berlin, 1996).
[4] G. Onida, L. Reining, and A. Rubio, Rev. Mod. Phys. **74**, 601 (2002), and references therein.
[5] J. M. Pitarke and A. G. Eguiluz, Phys. Rev. B **57**, 6329 (1998); **63**, 045116 (2001).
[6] J. F. Dobson and J. Wang, Phys. Rev. Lett. **82**, 2123 (1999).
[7] M. Lein, E. K. U. Gross, and J. P. Perdew, Phys. Rev. B **61**, 13 431 (2000).
[8] J. F. Dobson and J. Wang, Phys. Rev. B **62** 10 038 (2000).
[9] F. Furche, Phys. Rev. B **64**, 195120 (2001).
[10] M. Fuchs and X. Gonze, Phys. Rev. B **65**, 235109 (2002).
[11] F. Aryasetiawan, T. Miyake, and K. Terakura, Phys. Rev. Lett. **88**, 166401 (2002); M. Fuchs, K. Burke, Y. M. Niquet, and X. Gonze, *ibid.* **90**, 189701 (2003); F. Aryasetiawan, T. Miyake, and K. Terakura, *ibid.* **90**, 189702 (2003).
[12] T. Miyake, F. Aryasetiawan, T. Kotani, M. van Schilfgaarde, M.

Usuda, and K. Terakura, Phys. Rev. B **66**, 245103 (2002).
[13] J. M. Pitarke and J. P. Perdew, Phys. Rev. B **67**, 045101 (2003).
[14] B. Holm, Phys. Rev. Lett. **83**, 788 (1999).
[15] P. García-González and R. W. Godby, Phys. Rev. B **63**, 075112 (2001).
[16] P. García-González and R. W. Godby, Phys. Rev. Lett. **88**, 056406 (2002).
[17] R. W. Godby and P. García-González, in *A primer in Density Functional Theory*, edited by C. Fiolhais, F. Nogueira, and M. Marques (Springer, Berlin, 2003).
[18] N. E. Dahlen and Ulf von Barth, J. Chem. Phys. **120**, 6826 (2004); Phys. Rev. B **69**, 195102 (2004).
[19] W. Kohn and L. J. Sham, Phys. Rev. **140**, A1133 (1965).
[20] J. P. Perdew and Y. Wang, Phys. Rev. B **45**, 13 244 (1992).
[21] J. P. Perdew, K. Burke, and M. Ernzerhof, Phys. Rev. Lett. **77**, 3865 (1996).
[22] P. Sánchez-Friera and R. W. Godby, Phys. Rev. Lett. **85**, 5611 (2000).
[23] B. Holm and F. Aryasetiawan, Phys. Rev. B **62**, 4858 (2000).
[24] T. Miyake, F. Aryasetiawan, H. Kino, and K. Terakura, Phys. Rev. B **64**, 233109 (2001).
[25] H. Rydberg, M. Dion, N. Jacobson, E. Schröder, P. Hyldgaard, S. I. Simak, D. C. Langreth, and B. I. Lundqvist, Phys. Rev. Lett. **91**, 126402 (2003).
[26] Nonetheless, further XC effects are already introduced in the static KS system using, for instance, the local density approximation. Hence, in this context RPA means a random-phase approximation to calculate the response function but using the non-interacting KS response χ_0.
[27] J. F. Dobson, K. McLennan, A. Rubio, J. Wang, T. Gould, H. M. Le, and B. P. Dinte, Aust. J. Chem. **54**, 513 (2001), and references therein.
[28] Y. Andersson, D. C. Langreth, and B. I. Lundqvist, Phys. Rev. Lett. **76**, 102 (1996).
[29] M. Petersilka, U. J. Gossmann, and E. K. U. Gross, Phys. Rev. Lett. **76**, 1212 (1996).
[30] M. Corradini, R. Del Sole, G. Onida, and M. Palummo, Phys. Rev. B **57**, 14 569 (1998).
[31] M. Palummo, G. Onida, R. Del Sole, M. Corradini, and L. Reining, Phys. Rev. B **60**, 11 329 (1999).
[32] K. Tatarczyk, A. Schindlmayr, and M. Scheffler, Phys. Rev. B **63**, 235106 (2001).
[33] F. Sottile, V. Olevano, and L. Reining, Phys. Rev. Lett. **91**, 056402 (2003).
[34] A. Marini, R. Del Sole, and A. Rubio, Phys. Rev. Lett. **91**, 256402 (2003).
[35] C. F. Richardson and N. W. Ashcroft, Phys. Rev. B **50**, 8170 (1994).
[36] K. Utsumi and S. Ichimaru, Phys. Rev. B **22**, 5203 (1980).
[37] B. Farid, V. Heine, G. E. Engel, and I. J. Robertson, Phys. Rev. B **48**, 11 602 (1993).
[38] J. F. Dobson, Phys. Rev. Lett. **73**, 2244 (1994).
[39] J. Hubbard, Proc. R. Soc. London, Ser. A **243**, 336 (1957).
[40] A. Tsolakidis, E. L. Shirley, and R. M. Martin, Phys. Rev. B **69**, 035104 (2004), and references therein.
[41] D. M. Ceperley and B. J. Alder, Phys. Rev. Lett. **45**, 566 (1980).
[42] P. García-González, J. E. Alvarellos, E. Chacón, and P. Tarazona, Phys. Rev. B **62**, 16 063 (2000); Int. J. Quantum Chem., **91**, 139 (2002).
[43] J. Jung, P. García-González, J. E. Alvarellos, and R. W. Godby, Phys. Rev. A **69**, 052501 (2004).
[44] Z. Yan, J. P. Perdew, S. Kurth, C. Fiolhais, and L. Almeida, Phys. Rev. B **61**, 2595 (2000); Z. Yan, J. P. Perdew, and S. Kurth, *ibid.* **61**, 16 430 (2000).
[45] J. P. Perdew, H. Q. Tran, and E. D. Smith, Phys. Rev. B **42**, 11 627 (1987).
[46] H. B. Shore and J. H. Rose, Phys. Rev. Lett. **66**, 2519 (1991).
[47] J. F. Dobson and J. Wang, Phys. Rev. B **69**, 235104 (2004).
[48] J. M. Pitarke, Phys. Rev. B **70**, 087401 (2004).
[49] P. H. Acioli and D. M. Ceperley, Phys. Rev. B **54**, 17 199 (1996).
[50] E. Krotscheck and W. Kohn, Phys. Rev. Lett. **57**, 862 (1986).
[51] The explicit inclusion of the homogeneous response allows the evaluation of the homogeneous and inhomogeneous correlation energies in the same fashion. Thus, we eliminate important sources of errors due to not fully consistent comparisons of both energies.
[52] Of course, the exchange surface energy is the same for all the ACFDT approximation and it is calculated using the exact expressions.
[53] B. E. Sernelius and P. Björk, Phys. Rev. B **57**, 6592 (1998).
[54] P. M. Axilrod and E. Teller, J. Chem. Phys. **11**, 299 (1943); Y. Muto, Proc. Phys. Math. Soc. Jpn. **17**, 629 (1943).
[55] E. Engel, in *A primer in Density Functional Theory*, edited by C. Fiolhais, F. Nogueira, and M. Marques (Springer, Berlin, 2003), and references therein.
[56] Y. M. Niquet, M. Fuchs, and X. Gonze, J. Chem. Phys. **118**, 9504 (2003).
[57] A. G. Eguiluz, Phys. Rev. B **31**, 3303 (1985).
[58] J. F. Dobson, Phys. Rev. B **46**, 10 163 (1992).
[59] A. Liebsch, *Electronic Excitations at Metal Surfaces* (Plenum, New York, 1997).